Earth Syst. Sci. Data Discuss., https://doi.org/10.5194/essd-2018-46
Manuscript under review for journal Earth Syst. Sci. Data
Discussion started: 22 May 2018

Open Access Earth System Science Data Discussions

Generation and analysis of a new global burned area product based on MODIS 250m reflectance bands and thermal anomalies

Emilio Chuvieco[1], Joshua Lizundia-Loiola[1], M. Lucrecia Pettinari[1], Ruben Ramo[1], Marc Padilla[2], Kevin Tansey[2], Florent Mouillot[3], Pierre Laurent[4], Thomas Storm[5], Angelika Heil[6], Stephen Plummer[7]

[1] Environmental Remote Sensing Research Group, Department of Geology, Geography and the Environment, Universidad de Alcalá. Calle Colegios 2, Alcalá de Henares, 28801, Spain.
[2] Centre for Landscape & Climate Research, Leicester Institute for Space and Earth Observation, School of Geography, University of Leicester, Leicester LE1 7RH, United Kingdom
[3] UMR CEFE 5175, CNRS, Université de Montpellier,Université Paul-Valéry Montpellier, EPHE,IRD, 1919 route de Mende, 34293 Montpellier CEDEX 5, France
[4] Laboratoire des Sciences du Climat et de l'Environnement, CEA-CNRS-UVSQ, UMR8212, Gif-sur-Yvette, 91440, France
[5] Brockmann Consult GmBH, Max-Planck-Straße 2, D-21502 Geesthacht, Germany
[6] Max Planck Institute for Chemistry, Hahn-Meitner-Weg 1, B.3.53, 55128 Mainz, Germany.
[7] ESA Earth Observation Climate Office, ECSAT, Fermi Avenue Harwell Campus Didcot, Oxfordshire OX11 0FD United Kingdom.

Correspondence to: Emilio Chuvieco (emilio.chuvieco@uah.es)

Abstract. This paper presents a new global burned area (BA) product, generated from the MODIS red (R) and near infrared (NIR) reflectances and thermal anomalies data, thus providing the highest spatial resolution (approx. 250 m) among the existing global BA datasets. The product includes the full times series (2001-2016) of the MODIS archive. The BA detection algorithm was based on temporal composites of daily images, using temporal and spatial distance to active fires. The algorithm has two steps, the first one aiming to reduce commission errors by selecting the most clearly burned pixels (seeds), and the second one aiming to reduce omission errors by applying contextual analysis around the seed pixels. The product was developed within the European Space Agency's (ESA) Climate Change Initiative programme, under the Fire Disturbance project (Fire_cci). The final output includes two types of BA products: monthly full-resolution continental tiles (http://doi.org/cpk7) and biweekly global grid files at a degraded resolution of 0.25 degrees (http://doi.org/gcx9gf). Each one includes several auxiliary variables that were defined by the climate users to facilitate the ingestion of the product into global dynamic vegetation and emission models. The validation was based on a stratified random sample of 1200 pairs of Landsat images, covering the whole globe from 2003 to 2014. The estimated commission and omission error rates of the pixel product was 0.512 (0.020) and 0.708 (0.030), respectively, lower than previous ESA products but higher than the latest NASA MCD64A1 BA dataset. Examples of potential applications of this product to fire modelling based on burned patches analysis are included in this paper. They show greater sensitivity of our product to small burn patch detection than existing BA products.

Earth Syst. Sci. Data Discuss., https://doi.org/10.5194/essd-2018-46
Manuscript under review for journal Earth Syst. Sci. Data
Discussion started: 22 May 2018

1 Introduction

Biomass burning is one of the key processes affecting vegetation productivity, land cover, soil erosion, hydrological cycles and atmospheric emissions (Kloster and Lasslop, 2017; Forkel et al., 2017; Gaveau et al., 2014; van der Werf et al., 2017). It has social implications as well, impacting people's lives and properties (Roos et al., 2016), particularly in developed countries where urban areas are intermixed with forests (Bowman et al., 2017).

Fire is affected by climate, as burnings are associated with high to extreme weather conditions (particularly droughts and heatwaves) (Forkel et al., 2017). However, fire affects climate too, due to its impacts on carbon budgets and greenhouse gas emissions (van der Werf et al., 2017). These mutual influences between fire and climate explain that Fire Disturbance is considered one of the Essential Climate Variables (ECV) by the Global Climate Observing System (GCOS) program (Mason et al., 2010). Several space agencies are working on developing systematic assessments of fire occurrence and fire impacts, as part of their efforts to improve the use of satellite data in climate modelling. This is the main purpose of the Fire_cci project (http://www.esa-fire-cci.org/ last accessed March, 2018), which is part of the European Space Agency's (ESA) Climate Change Initiative (CCI) programme (Hollmann et al., 2013). The Fire_cci project aims to develop long term time series of burned area (BA) products adapted to the needs of climate modellers (Chuvieco et al., 2016). In addition to global BA products, the Fire_cci project is generating a small fire database for the African continent based on medium-resolution sensors on board the Sentinel-2 and Sentinel-1 satellites.

Global BA information is required for many different applications (Mouillot et al., 2014). First, it helps to assess fire risk assessment, by comparing estimated risk conditions with actual fire occurrence (Marlier et al., 2013; Chuvieco et al., 2014). Burned area information is also a critical input of Global Dynamic Vegetation Models, as it provides an estimation of carbon emissions and vegetation succession (Lasslop et al., 2014). In conjunction with other human and physical variables, BA datasets are required to understand factors controlling fire activity (Forkel et al., 2017) and particularly those affecting changes in fire regimes (Hantson et al., 2015; Andela et al., 2017), with an increasing concern on fire patch identification derived from higher resolution pixel-level information (Nogueira et al., 2017). Atmospheric emission models require precise information on spatio-temporal patterns of fire occurrence, as well as combustion characteristics (van der Werf et al., 2017; Knorr et al., 2016). Finally, BA information is needed to model fire impacts on human health (Reid et al., 2016) and safety of human properties (Moritz et al., 2014; Sturtevant et al., 2009).

A few global BA products have been developed in the last years. Two sensors have been particularly used to develop these global BA time series datasets: VEGETATION (VGT), on board the SPOT satellites since 1998, and MODIS, on board the Terra and Aqua satellites since 2000. The former images have been used to create BA products funded under different European projects: L3JRC (Tansey et al., 2008), Globcarbon (Plummer et al., 2005) and Copernicus GIO_GL1_BA BA products, all at 1000 m spatial resolution (after 2013 this product is available at 333 m resolution and is derived from PROBA-V data). The MODIS sensor has been used to generate two NASA's global BA time series, the MCD45A1 and the MCD64A1. Both provide BA detections at 500m from 2000 to the present. The MCD45A1 is derived from a change

detection algorithm based on a bi-directional reflectance model (Roy et al., 2008), while the MCD64A1 is derived from a hybrid algorithm that uses both the reflectance changes and the thermal anomalies associated to biomass burning (Giglio et al., 2009). The latest version of this algorithm is the basis for the now standard MODIS BA product collection 6 (http://modis-fire.umd.edu/pages/BurnedArea.php?target=Download, last accessed March, 2018). From the BA detections of the MCD64A1 product with additional variables on fuel properties and emission coefficients, the Global Fire Emissions Database (GFED) was created. Current versions of the GFED (named 4 and 4s) include information from the MCD64A1 collection 5 product as well as from the ATSR sensor (on board the ERS satellites) for the pre-MODIS era (1995-2000). The GFED 4s adds an estimation of the area burned by small fires (not detected by the standard MODIS product), which is derived from the relation between number of hotspots and burn patches (van der Werf et al., 2017).

Finally, ENVISAR MERIS images have also been used for generating global BA products, with a shorter time series than VGT and MODIS (just for the period when MERIS archives provide enough input data: 2005-2011), but with higher spatial resolution (300m) (Chuvieco et al., 2016; Alonso-Canas and Chuvieco, 2015).

This paper aims to present a new global BA product based on the highest spatial-resolution bands of the MODIS sensor (bands 1 and 2 at approximately 250m). The goal of generating this product was to complement existing BA products generated from the 500m MODIS bands, as well as to improve detection rate of smaller burn patches. The paper describes the BA algorithm used for generating the BA products, presents a spatio-temporal validation of the results and describes examples of BA analysis for fire-related climate models, which should benefit from higher spatial resolution of BA detections.

2 Methods

2.1 Algorithm design

The main input for running the BA algorithm was the MOD09GQ collection 6 reflectance product. It includes the daily red (R) and near infrared (NIR) corrected reflectances of the Terra-MODIS bands 1 and 2, respectively, both at approximately 250 m resolution in sinusoidal projected tiles of 1200x1200 km. Pixel quality information was obtained from MOD09GA product, as recommended by the MODIS Science team (https://lpdaac.usgs.gov/dataset_discovery/modis/modisproducts_table/mod09gq_v006, last accessed March 2018). Additionally, the algorithm used the MODIS thermal anomalies product (MCD14ML collection 6), which includes active fires (named here hotspots, HS), detected from the sensor's middle infrared and thermal channels (Giglio et al., 2016).

The MOD09GQ 250m product includes atmospheric corrections, but it does not contain BRDF corrections, which is an important source of reflectance variability, particularly for BA detection, as the reflectance change caused by the fire might be lower than the one caused by the angular effects (Roy et al., 2005). For this reason, several BRDF correction models were tested, but none reported satisfactory results, as they greatly smoothed the burned signal in some biomes. As an alternative to obtain a consistent time series, monthly composites of daily reflectance were created. Pixels with low quality observations

Earth Syst. Sci. Data Discuss., https://doi.org/10.5194/essd-2018-46
Manuscript under review for journal Earth Syst. Sci. Data
Discussion started: 22 May 2018

(cloud, cloud shadows) taken from MOD09GA QA were discarded before compositing. Unburnable pixels were discarded too. They comprised water, bare areas, permanent snow and ice and urban areas. This information was derived from the Land Cover CCI Product version 1.6.1, using 3 epochs corresponding to 2000, 2005 and 2010, and at a similar spatial resolution of approx. 300 m (Kirches et al., 2013).

The criterion to create the monthly composites was based on the HS dating. It was assumed that the closest day to the nearest hotspot would be the most adequate to obtain the post-fire reflectances. Although composites include 30 days, for areas with HS dated at the latest days of the monthly period, ten extra running dates (including images from the next month) were used to have enough post-fire observations for creating the composites. After creating Thiessen polygons with the HS location and labelling them with the HS date, the algorithm selected the closest date to the three minimum NIR monthly reflectances. The actual date was selected based on whether the three minimum NIR values occurred before or after the HS date. If all three were acquired before or after the HS date, the date of the second lowest was selected. In this way, clouds shadows or smoke not included in the QA would not affect the composite. When one or two were acquired after the HS, the closest date to the HS' was selected. Finally, the monthly composites were generated taken the R and NIR reflectances for the selected dates. From these two bands, the Global Environmental Monitoring Index (GEMI: Pinty and Verstraete, 1992) was computed as:

$$GEMI = \eta(1 - 0.25\eta) - \frac{(\rho_{Red} - 0.125)}{1 - \rho_{Red}}, \quad (1)$$

$$\eta = \frac{2(\rho_{NIR}^2 - \rho_{Red}^2) + 1.5\rho_{NIR} + 0.5\rho_{Red}}{\rho_{Red} + \rho_{NIR} + 0.5}, \quad (2)$$

where ρ_{NIR} is the NIR reflectance (band 2 of the MOD09GQ product) and ρ_R the R reflectance (band 1). This index has been previously used in burned area detection from R and NIR channels (Barbosa et al., 1999; Chuvieco et al., 2002; Pereira, 1999).

The BA algorithms followed a two-phase approach, detecting in the first phase the most clearly burned pixels (named seeds) and improving the burn shape detection in the second one using a contextual analysis around the seed pixels. The former phase aims to reduce the commission errors, while the latter the omission errors. This approach has been widely used in BA detection algorithms (Alonso-Canas and Chuvieco, 2015; Bastarrika et al., 2011; Chuvieco et al., 2008). In addition, the algorithm is spatially adaptable, as it collects statistics from each MODIS tile to generate the detection thresholds.

The seed phase begun with positioning the HS within a 5x5 pixel window, as the HS product has 1000 m resolution and the MOD9GQ has 250 m resolution. The pixel with the minimum NIR within each window was selected as the best candidate for having a recent burn. Cumulative Distribution Functions (CDF) of unburned and potentially burned areas were created to define adaptive thresholds to cope with the wide variety of global fire conditions. To reduce potential noises, HS were only considered as potential burns when the NIR was lower than the previous month and the NIR value was lower than the 10% threshold of the unburned pixels' CDF. Seeds were considered as those having a low NIR value (extracted from the CDF of potential burns), a decrease in NIR value, and at least one HS in the surrounding 3x3 pixel window.

The growing phase included several criteria to add new burned pixels to each burn patch created in the first phase. Within each iteration, candidate pixels had to be neighbours of seed burns (or burned pixels detected in the previous iteration), having a NIR value below a CDF threshold of the potentially burned pixels, and showing a decrease in NIR values from the previous month. In this growing phase, an additional threshold based on the CDFs of GEMI values (Eq. (1)) for burned and unburned areas was also used. The process was iterated until no further pixels were added to each burn patch. Finally, a morphological filter with two steps of erosion-dilatation was applied to eliminate small patches of burned pixels or small islands of unburns within burned patches.

2.2 Product specifications

As the result of a user requirement analysis, two BA products (pixel and grid) were generated within the Fire_cci v5.0 project. Both were reprojected to geographical coordinates. The former included the date of detection (0-366), the uncertainty of the estimation (0-100) and the land cover affected by the fire (taken from the Land Cover CCI product of a similar time period). Pixel products had the full resolution of the MODIS input images (231.65 m). Monthly files were generated to avoid missing double burns in a single year. The output datasets were created as GEOTIFF format and comprised quasi-continental tiles (Table 1).

The grid product was produced for biweekly periods and incorporated 23 layers at 0.25 degree resolution: sum of burned area (m^2), standard deviation of the estimation (m^2), fraction of burnable area (0-1), fraction of observed area (0-1), number of burned patches (0-N), and sum of burned area in 18 land cover classes (again taken from the Land Cover CCI product). The output datasets are NetCDF-CF (http://www.unidata.ucar.edu/software/netcdf/docs, last accessed March 2018).

The uncertainty layer estimated the probability that each pixel was correctly classified as burned. It was derived from four input layers related to the BA detection algorithm: the number of daily images to build the monthly composite, the percentile of the NIR reflectance in the CDF of burned and unburned pixels, the CDF of the GEMI differences and the distance to the closest HS. These variables were normalized and combined to obtain the pixel confidence level, from which the standard error of the grid product was calculated. The fraction of burnable area was computed from the land cover CCI product, while the fraction of observed area from the monthly integrated QA values. The burn patches were computed considering as a patch a group of contiguous burned pixels having burn detection date differences shorter than 15 days. This criterion has been commonly used for global characterization of burned patches (Hantson et al., 2015).

2.3 Validation methods

The accuracy assessment was based on a stratified random sample of reference data distributed across the globe and throughout twelve years, 2003-2014. For comparison purposes, additionally to the product version presented here, the validation analysis included a previous Fire_cci product version, v4.1 (Chuvieco et al., 2016), based on MERIS images, and the MCD64A1 c6.

Reference data were generated from pairs of medium resolution satellite images as recommended by the CEOS-CalVal protocol (Boschetti et al., 2009). Burned patches observed between pairs of Landsat images were mapped with a semi-automatic classification algorithm. The classification made by one interpreter was systematically reviewed by another. Any errors were rectified and the revision repeated iteratively until no new errors were detected.

The sampling units were defined spatially by the Thiessen scene areas (TSAs) constructed by Cohen et al. (2010) and Kennedy et al.(2010), and temporally by the dates of Landsat imagery available. The population of sampling units was stratified by calendar years, the biomes as defined by Olson et al. (2001) and BA as detected by GFED. Each year-biome stratum was divided in two parts using BA thresholds designed to minimize the expected variance of BA given the available sample size. The yearly sampling size was fixed to one-hundred (for twelve years, 1200 in total) and was allocated across strata proportionally to GFED BA data. Details on comparisons between several options of stratification and sample allocation can be found in Padilla et al. (2017).

Each sampling unit selected was subsampled by a spatial cluster of pixels on a 30km x 20km window. This subsampling stage allowed reducing the amount of reference data generated for a given year. This, in turn, allowed expanding the probability sampling design to a multi-year period (twelve years), for the first time in global BA validation.

Accuracy metrics, based on the error matrix approach (Congalton and Green, 1999), were computed. Since the burned category is much less frequent that the unburned, the overall accuracy was not taken into account, as it was very influenced by the unburned pixels classification. Instead, the omission and commission errors were computed, as well as the Dice Coefficient (DC) and the relative bias of the burned category. The DC is defined as the probability that one classifier (product or reference data) identifies a pixel as burned given that the other classifier also identifies it as burned (Fleiss, 1981). Relative bias was computed as the ratio of the difference between omission and commission errors and the true burned pixels. The formulas of accuracy measures can be found in Padilla et al. (2015). The details of the sampling design and the formulas used to infer accuracy at global scale can be found in the validation report of the Fire_cci Phase 2 project (Padilla et al., in preparation).

2.4 Product intercomparison

Spatial and temporal trends of the MODIS Fire_cci v5.0 were compared with existing global BA products. We selected three products currently operational: the GFED4, widely used for fire emissions, which is based on the MODIS MCD64 c5; the MCD64 c6, now the standard NASA BA product, and the MERIS Fire_cci v4.1, with a shorter time series (2005-2011). Global temporal trends of these products were generated. Spatial comparison between products was performed at 0.25-degree resolution.

2.5 Product assessment

As an example of potential uses of the MODIS Fire_cci v5.0 product in fire models, the pixel-level product was analysed based on the spatio-temporal aggregation of burned pixels into fire patches. The variables investigated were (i) the ability of

the medium spatio-temporal resolution to identify individual fire patches and capture their size distribution following the self- criticality hypothesis (Hantson et al., 2015), and (ii) how the resulting fire patch shape improves with finer resolution to better capture spreading processes and impacts on post-fire vegetation dynamic as proposed by Nogueira et al. (2017) and Chuvieco et al. (2016) for pixel-level global remote sensing product assessment. MODIS Fire_cci v5.0 (approx. 250 m resolution) was compared with MCD64A1 c6 (approx. 500 m resolution) at the global level, and with the Sentinel 2 (20 m) BA product generated within the Fire_cci project for Northern Hemisphere Tropical Africa. Individual fire-shape indices were defined as the ratio between log perimeter and the square root of the area.

For comparison, difference maps between MODIS Fire_cci v5.0 and MCD64A1 c6 were computed. Fire size distribution was characterized by the slope β of the fire number to fire size relationship (log scale). The slope was adjusted using the same methodology as in Laurent et al. (Laurent et al., 2018 submitted). Grid-cell to grid-cell correlations accounting for spatial autocorrelation of both products were implemented with a modified t test of spatial association based on Clifford et al. (1989) and Dutilleul et al. (1993), and performed with the modified.ttest function of the 'SpatialPack' R cran package (https://CRAN.R-project.org/package=SpatialPack, last accessed March, 2018). In order to compare the same fire size category between the two products, a threshold of 107 ha was applied on fire size. This threshold corresponds to the size of a 5-pixel fire patch at equator for the MCD64A1 c6 product.

3 Results

3.1 Burned area trends

The MODIS Fire_cci v5.0 BA product includes the global time series from 2001 to 2016. Average yearly BA was 3.808 Mkm^2. Years with largest BA were 2004, 2011 and 2012 with more than 4 Mkm^2 each, while only 2013 and 2016 had less than 3.5 Mkm^2. Figure 1 shows the spatial distribution of average annual BA of the full time series. The tropical belts of Africa, America and Australia were the most extensively burned, particularly the former. Temperate forest in Western Europe and US, grasslands and croplands of South SE Asia, Far East Russia, and northern Kazakhstan had also significant fire occurrence.

Persistent burnings occur mostly in Tropical regions, which have large BA throughout the time series. Figure 2 shows the coefficient of variation of the yearly BA for the whole time series. High values indicate regions where fire occurrence is less regular, which is commonly associated to longer fire return intervals. This is the case of the boreal latitudes (Canada, Alaska, and Russia) and many temperate regions (most US, and the southern regions of Europe, Africa, Australia and Latin America).

The most persistent biomass burnings occur in tropical mainland Africa and Madagascar (excluding the rainforest), northern Australia and tropical Latin America (both Hemispheres), excluding the central Amazonian region and the Andes. Fire persistency is also observed in large agricultural areas of southern Russia, US and SE Asia (Myanmar, Laos, Thailand and Vietnam).

Earth Syst. Sci. Data Discuss., https://doi.org/10.5194/essd-2018-46
Manuscript under review for journal Earth Syst. Sci. Data
Discussion started: 22 May 2018

3.2 Comparison with existing products

Figure 3 shows the temporal trends of global BA (in km^2) estimated from several existing global BA products. The MODIS Fire_cci v5.0 provided an intermediate estimation between the MCD64 c6 and the GFED4 BA products. It was similar to the MERIS Fire_cci v4.1 for the 2007-2009 years, but showed larger estimations for 2010 and 2011, because of the limited availability of MERIS images for those two years.

Trends in BA derived from these products are remarkably similar among the years, with a stable behaviour at the beginning of the time series and a trend towards slight decrease starting from 2007. The MERIS Fire_cci v4.1 product showed a high decline in 2010, caused by the lack of observations in the last years of the time series. For this reason, and for being derived from a different sensor, the correlation of annual estimates of MERIS Fire_cci v4.1 with the MODIS Fire_cci v5.0 product is much lower (r^2=0.12) than for the other MODIS based products (r^2>0.79 in both cases: Fig. 4). The annual estimations of the MODIS Fire_cci v5.0 product were lower than for the MCD64A1 c6 by 11% and higher than for MERIS Fire_cci v4.1 (10%) and GFED4 (12%) products.

In terms of global spatial patterns of annual BA, MODIS Fire_cci v5.0 shows a higher agreement with MODIS based products than with the MERIS Fire_cci product v4.1 (Fig. 5 and Table 2). The average determination coefficient (r^2) of the pairwise correlation of MODIS Fire_cci v5.0 with the MODIS products MCD64A1 c6 and GFED4 is 0.70 and 0.67, respectively, and exhibits only little inter-annual variability across 2005 to 2011. The spatial agreement with the MERIS Fire_cci product is strongly dependent on the year. While r^2 values range between 0.63 and 0.65 in the years 2005 to 2009, they are distinctively lower in 2010 (r^2=0.44) and 2011 (r^2=0.54), which again should be related to the lack of MERIS observations in those years. Table 2 also highlights that the global spatial BA patterns of GFED4 and MCD64A1 c6 are largely similar (average r^2=0.93) despite global annual burned area increased by 27% with the update of MCD64A1 from c5 to c6 (see also Fig. 4).

3.3 Product validation results

The accuracy of MODIS Fire_cci v5.0 product, expressed by a Dice coefficient (DC) value of 0.365 (standard error = 0.026) was significantly higher than for the MERIS Fire_cci v4.1 product (DC=0.248 with SE= 0.030), but lower than for the MCD64A1 c6 product (DC=0.478 with SE=0.031). The validation was based on the time series when reference data were available (2003-2014: Fig. 6). Global commission and omission error ratios (Ce and Oe) were 0.512 (0.020) and 0.708 (0.30) for the MODIS Fire_cci v5.0 product, with lower commission values (around 0.4) for 2007, 2009, 2011 and 2012. The same years have also lower omission errors (<0.6). The MERIS Fire_cci v4.1 had a total of 0.643 (0.045) omission and 0.810 (0.030) commission rates, while the MCD64A1 c6 had 0.353 (0.016) and 0.622 (0.038), respectively. MODIS Fire_cci v5.0 underestimates a fraction of 0.402 (0.058) of the BA reported in the reference sample, as expressed by the relative bias (relB), slightly less than MCD64A1 c6, 0.415 (0.056), and lower than MERIS Fire_cci v4.1, 0.468 (0.094). From this point of view the MODIS Fire_cci v5.0 product is better equilibrated than the other BA products.

Earth Syst. Sci. Data Discuss., https://doi.org/10.5194/essd-2018-46
Manuscript under review for journal Earth Syst. Sci. Data
Discussion started: 22 May 2018

Estimated accuracy values include errors related to date reporting accuracy and those caused by burns smaller than the pixel size, and therefore it may be considered a pessimistic estimation of accuracy. In fact, average commission and omission errors were much lower for three large study sites located in North Australia, Central Canada and California (>0.5 Mkm2 each) from which national fire perimeters were available (see details in Chuvieco et al., 2016). In these cases, using data from 2008, omission and commission errors were estimated at 0.15 and 0.23, respectively, similar to those obtained for the MCD64 c6 (0.14 and 0.23, respectively) and lower than for GFED4 (0.12 and 0.30, respectively) and MERIS Fire_cci v4.1 (0.18 and 0.44, respectively).

The temporal trends of accuracies are remarkably similar among products. Relative differences between products accuracies observed in one year are similarly replicated on the other years (Fig. 6). Yearly accuracies are estimated with relatively low precision (large 95% confidence intervals) and show relatively high inter-annual variability without clear monotonic trends.

Accuracy of MODIS Fire_cci v5.0 tended to be highest across the tropical and subtropical savannah of Africa, South America and Australia, where fire occurrence was high (Fig. 7), and decreased in temperate forest and croplands. BA was commonly underestimated (relB<0).

3.4 Fire patch analysis

Figure 8 displays the global pattern of fire patch density (number of fire patches/km^2) calculated from the MODIS Fire_cci v5.0 and MCD64A1 c6 products. A similar global pattern was observed for both datasets, with the savannas and temperate grasslands yielding higher fire patch density. When plotting the difference between the two products, it was observed that MODIS Fire-cci v5.0 detected more fire patches in woody savannas and open shrubland/grasslands worldwide (+52%), while it detected less fire patches in savannas (-42%). In other biomes, no clear spatial pattern was observed, with a mixture of fire patch densities varying +/- 70%. The total number of fire patches without and with considering a 107 ha fire size threshold estimated globally for MODIS Fire_cci v5.0 was 1.20×10^6 and 0.54×10^6, respectively. This last number reached 0.56×10^6 for MCD64A1 c6. Therefore, when considering a minimum fire patch size threshold of 107 hectares, it was observed a difference of 3.7% between the two products, indicating that the 250 m resolution doubles fire patch number by accounting smaller ones, and kept almost constant the total number of large fire patches with only local differences. The grid-cell-to-grid-cell correlation between the two products was high for fire patch number with $r^2=0.932$ (p-value <<0.01). When comparing with Sentinel 2 data over northern hemisphere Africa, the obtained values were $r^2=0.839$ (p<<0.01) for MODIS Fire_cci v5.0 and $r^2=0.836$ for MCD64A1 c6 (p<<0.01).

The slope β of the fire number/fire size relationship (log scale) is presented in Fig. 9 for each product for the period 2001-2016, alongside their uncertainties. It was observed a similar global spatial pattern between the two products and values varying between 0.4 and 1.8. However, a steeper slope was also observed (higher beta, Δ=+0.15 on average) of the fire size distribution in MODIS Fire_cci v5.0, indicating that small fires were more frequent. This observation is particularly important and systematic in savannas, with the highest positive differences observed in South America (Δ=+0.4). A reverse

pattern was observed in grasslands with a flatter slope in MODIS Fire_cci v5.0 (Δ=-0.25). As a result, the level of agreement is good at global scale, except for the regions mention above.

Grid-cell-to-grid-cell correlations of the β slope between MODIS Fire_cci v5.0 and MCD64A1 c6 were high, with r^2=0.84 ($p<<0.01$) when considering fire size larger than the 107 ha and grid cells with p-value <0.01 for the significance of the fire size/fire number relationship in each product. When comparing with Sentinel 2 data for Northern Hemisphere Africa, the obtained grid-cell-to-grid-cell relationship had a r^2= 0.49 (p=0.0073) for MODIS Fire_cci v5.0, and a little lower with r^2= 0.36 (p=0.033) for MCD64A1 c6 when selecting a fire size larger than 107 ha and grid cells with a p-value <0.025 for the significance of the fire size/fire number relationship. Lower correlations with Sentinel-2 might result from the smaller time frame (2016-2017) used for this sensor.

The pixel-level characterization of fire patches was also used to extract their shape index (SI) information. As an example of pixel-level product use and the derived fire patches, fire shapes show the drivers of fire spread as wind-driven fires would be more elongated than fire spreading under mild conditions. Fire shape complexity can also show the difficulty of the fire to spread over fragmented landscapes or complex topography (Hargrove et al., 2000; Cary et al., 2006). On the other side, fire shape complexity can provide keystone information on fire refugia of unburned islands within or at the boundary of fire patches (Román-Cuesta et al., 2009). Figure 10 illustrates the mean fire shape index (SI) from MODIS Fire_cci v5.0 and MCD64A1 c6 for the 2000-2016 period. A minimum shape fire complexity was observed in savannas and tropical forests, with a highest complexity in the boreal forests and grasslands. The global pattern of fire complexity is conserved between the two products, with a systematic higher and more precise characterization of the complexity in the MODIS Fire_cci v5.0 product, because of its higher spatial resolution. The global grid-cell-to-grid-cell correlation analysis of SI reached r^2= 0.528 ($p<<0.01$) between the two products. When correlating SI values from the MODIS Fire_cci v5.0 product with the Sentinel-2 BA product for Northern Hemisphere Africa, a value of r^2=0.3 ($p<0.01$) was obtained with no fire size threshold and r^2=0.111 (p=0.017) when fire patch size is larger than 107 ha. A similar correlation (r^2=0.111, p=0.01) was obtained for MCD65A1 c6 when selecting fire patches larger than 107 ha, while the correlation without this fire size threshold was lower (r^2=-0.004, p=0.9), indicating the benefit of the higher spatial resolution of MODIS Fire_cci v5.0, as it captures the shape of smaller fires and provides better agreement with the fine scale resolution of Sentinel-2 data.

4. Discussion

This paper has presented a new global BA product aimed to improve the information available to climate modellers on spatio-temporal patterns of fire occurrence. The MODIS Fire_cci is the first global BA product derived from the two highest spatial resolution channels (R, NIR) of this sensor, with approximately 250 m pixel size. This made this product theoretically more suitable to analyse spatial properties of burned patches than other existing global BA datasets. The first assessment of the product apparently confirms this hypothesis, as it is more sensitive than the MCD64A1 c6 product to detect small fire patches, when both were compared to BA products derived from Sentinel-2 (20 m pixel size) in the African continent.

With respect to spatial and temporal variability, the MODIS Fire_cci v5.0 BA product provides similar trends to the MCD64A1 c6, showing the highest fire occurrence in dry Tropical regions of Africa, Australia and South America. Global estimates of BA for MODIS Fire_cci v5.0 product range from 3.24 Mkm^2 of 2013 to 4.16 Mkm^2 of 2011, with a slight trend towards declining the total BA in the whole period (2001-2016). This follows other observations of global BA trends (Andela et al., 2017), particularly evident in the last 4 years.

Comparison of our results with the standard NASA BA product (MCD64A1 c6) showed similar accuracy for the three calibration sites where fire perimeters were available (Australia, Canada and California). However, globally speaking the average accuracy estimated for the MODIS Fire_cci v5.0 product was lower than for the MCD64A1 c6 product, particularly in terms of omission errors. It should be pointed out that the recently released c6 version has significantly increased the detection of fire patches with respect to previous MCD64A1 versions (around 30% more BA than c5, which is the basis of GFED4). The main advantage of the MCD64A1 over our product is the use of SWIR bands, which have been widely reported as very sensitive to BA detection (Bastarrika et al., 2011; Giglio et al., 2009; Martín et al., 2005). However, this implies reducing four times the spatial resolution of the MODIS Fire_cci v5.0 product. Further efforts are required for achieving higher accuracy metrics, while keeping the higher resolution data of the R-NIR bands. In addition to the MODIS sensor, BA algorithms based on just NIR bands would also benefit from having higher spatial resolution than SWIR bands in other sensors, such as OLCI or VIIRS. Improved resolution of BA products is clearly relevant for fire modellers, as it has been shown with the example of the fire patch analysis. Compared with other existing products, the MODIS Fire_cci v5.0 product provides higher accuracy values than previous Fire_cci versions (based on MERIS data), as well as other European BA products based on SPOT-VEGETATION images.

5. Data availability

The Fire_cci products are freely available through the Fire_cci website (www.esa-fire-cci.org, last accessed March 2018), or through the CCI Open Data Portal (http://cci.esa.int/data, last accessed March 2018). To receive updates on the products and information on new datasets, users are encouraged to register with the Fire_cci project at https://geogra.uah.es/fire_cci/ (last accessed March 2018).

6. Conclusions

This paper has presented the MODIS Fire_cci v5.0 BA product. It is based on MODIS bands R and NIR bands, thus providing the highest spatial resolution of existing global BA datasets (approx. 250 m), The BA algorithm follows a two-phase approach, detecting first the core burned pixels and after applying a contextual analysis to discriminate the burn patch. Information from thermal anomalies was used to define probability functions adapted to spatio-temporal variation of fire activity. The algorithm was used to process the 2001-2016 MODIS time series. Two set of products were generated: pixel (at

full resolution), with date of detection, confidence level and land cover, and grid (at 0.25 degree resolution), with BA, standard error, fraction of observed area, fraction of burnable area, number of patches, and BA for 18 different land covers.

Competing interests

The authors declare that they have no conflict of interest.

Author Contribution

Emilio Chuvieco is the Science Leader of the Fire_cci project and has coordinated the manuscript production and supervised the BA algorithm, Joshua Lizundia-Loiola, M. Lucrecia Pettinari and Ruben Ramo developed the BA algorithm and contributed to the writing, Marc Padilla and Kevin Tansey performed the validation and contributed to the writing, Florent Mouillot and Pierre Laurent performed the burned patch analysis and contributed to the writing, Thomas Storm was in charge of data processing, Angelika Heil did the intercomparison analysis and contributed to writing, and Stephen Plummer is the Technical Officer of ESA and contributed with project ideas and manuscript writing.

Acknowledgements

This study has been funded by the ESA Fire_cci project, which is part of the ESA Climate Change Initiative Programme.

References

Alonso-Canas, I., and Chuvieco, E.: Global Burned Area Mapping from ENVISAT-MERIS data RSE, 163, 140-152, Doi: http://dx.doi.org/10.1016/j.rse.2015.03.011, 2015.

Andela, N., Morton, D. C., Giglio, L., Chen, Y., van der Werf, G. R., Kasibhatla, P. S., DeFries, R. S., Collatz, G. J., Hantson, S., Kloster, S., Bachelet, D., Forrest, M., Lasslop, G., Li, F., Mangeon, S., Melton, J. R., Yue, C., and Randerson, J. T.: A human-driven decline in global burned area, Science, 356, 1356-1362, Doi: 10.1126/science.aal4108, 2017.

Barbosa, P. M., Grégoire, J. M., and Pereira, J. M. C.: An algorithm for extracting burned areas from time series of AVHRR GAC data applied at a continental scale, RSE, 69, 253-263, 1999.

Bastarrika, A., Chuvieco, E., and Martín, M. P.: Mapping burned areas from Landsat TM/ETM+ data with a two-phase algorithm: balancing omission and commission errors, RSE, 115, 1003-1012, 2011.

Boschetti, L., Roy, D. P., and Justice, C. O.: International Global Burned Area Satellite Product Validation Protocol. Part I – production and standardization of validation reference data, http://lpvs.gsfc.nasa.gov/DOC/protocol_revised_Apr09.doc, 2009.

Bowman, D. M., Williamson, G. J., Abatzoglou, J. T., Kolden, C. A., Cochrane, M. A., and Smith, A. M.: Human exposure and sensitivity to globally extreme wildfire events, Nature Ecology & Evolution, 1, 0058, 2017.

Cary, G. J., Keane, R. E., Gardner, R. H., Lavorel, S., Flannigan, M. D., Davies, I. D., Li, C., Lenihan, J. M., Rupp, T. S., and Mouillot, F.: Comparison of the sensitivity of landscape-fire-succession models to variation in terrain, fuel pattern, climate and weather, Landscape Ecology, 21, 121-137, 2006.

Clifford, P., Richardson, S., and Hémon, D.: Assessing the significance of the correlation between two spatial processes, Biometrics, 123-134, 1989.

Cohen, W. B., Yang, Z., and Kennedy, R.: Detecting trends in forest disturbance and recovery using yearly Landsat time series: 2. TimeSync — Tools for calibration and validation, RSE, 114, 2911-2924, Doi: http://dx.doi.org/10.1016/j.rse.2010.07.010, 2010.

Congalton, R. G., and Green, K.: Assessing the Accuracy of Remotely Sensed Data: Principles and Applications, Lewis Publishers, Boca Raton, 137 pp., 1999.

Chuvieco, E., Martín, M. P., and Palacios, A.: Assessment of different spectral indices in the red-near-infrared spectral domain for burned land discrimination, IJRS, 23, 5103-5110, 2002.

Chuvieco, E., Englefield, P., Trishchenko, A. P., and Luo, Y.: Generation of long time series of burn area maps of the boreal forest from NOAA–AVHRR composite data, RSE, vol. 112, 2381-2396, Doi: doi:10.1016/j.rse.2007.11.007, 2008.

Chuvieco, E., Aguado, I., Jurdao, S., Pettinari, M. L., Yebra, M., Salas, J., Hantson, S., de la Riva, J., Ibarra, P., Rodrigues, M., Echeverría, M., Azqueta, D., Román, M. V., Bastarrika, A., Martínez, S., Recondo, C., Zapico, E., and Martínez-Vega, F. J.: Integrating geospatial information into fire risk assessment, IJWF, 23, 606–619, Doi: http://dx.doi.org/10.1071/WF12052, 2014.

Chuvieco, E., Yue, C., Heil, A., Mouillot, F., Alonso-Canas, I., Padilla, M., Pereira, J. M., Oom, D., and Tansey, K.: A new global burned area product for climate assessment of fire impacts, Global Ecology and Biogeography, 25, 619-629, Doi: 10.1111/geb.12440, 2016.

Dutilleul, P., Clifford, P., Richardson, S., and Hemon, D.: Modifying the t test for assessing the correlation between two spatial processes, Biometrics, 305-314, 1993.

Fleiss, J. L.: Statistical methods for rates and proportions, John Wiley & Sons, 1981.

Forkel, M., Dorigo, W., Lasslop, G., Teubner, I., Chuvieco, E., and Thonicke, K.: A data-driven approach to identify controls on global fire activity from satellite and climate observations (SOFIA V1), Geoscientific Model Development, 10, 4443-4476, Doi: https://doi.org/10.5194/gmd-10-4443-2017, 2017.

Gaveau, D. L., Salim, M. A., Hergoualc'h, K., Locatelli, B., Sloan, S., Wooster, M., Marlier, M. E., Molidena, E., Yaen, H., and DeFries, R.: Major atmospheric emissions from peat fires in Southeast Asia during non-drought years: evidence from the 2013 Sumatran fires, Scientific reports, 4, 2014.

Giglio, L., Loboda, T., Roy, D. P., Quayle, B., and Justice, C. O.: An active-fire based burned area mapping algorithm for the MODIS sensor, RSE, 113, 408-420, 2009.

Giglio, L., Schroeder, W., and Justice, C. O.: The collection 6 MODIS active fire detection algorithm and fire products, RSE, 178, 31-41, 2016.

Hantson, S., Pueyo, S., and Chuvieco, E.: Global fire size distribution is driven by human impact and climate, Global Ecology and Biogeography, 24, 77-86, Doi: 10.1111/geb.12246, 2015.

Hargrove, W. W., Gardner, R., Turner, M., Romme, W., and Despain, D.: Simulating fire patterns in heterogeneous landscapes, Ecological Modelling, 135, 243-263, 2000.

Hollmann, R., Merchant, C. J., Saunders, R., Downy, C., Buchwitz, M., Cazenave, A., Chuvieco, E., Defourny, P., de Leeuw, G., and Forsberg, R.: The ESA climate change initiative: Satellite data records for essential climate variables, B Am Meteorol Soc, 94, 1541-1552, 2013.

Kennedy, R. E., Yang, Z., and Cohen, W. B.: Detecting trends in forest disturbance and recovery using yearly Landsat time series: 1. LandTrendr — Temporal segmentation algorithms, RSE, 114, 2897-2910, Doi: http://dx.doi.org/10.1016/j.rse.2010.07.008, 2010.

Kirches, G., Krueger, O., Boettcher, M., Bontemps, S., Lamarche, C., Verheggen, A., Lembrée, C., Radoux, J., and Defourny, P.: Land Cover CCI: Algorithm Theoretical Basis Document Version 2, Land_Cover_CCI_ATBDv2_2.3, Louvain, Belgium, 2013.

Kloster, S., and Lasslop, G.: Historical and future fire occurrence (1850 to 2100) simulated in CMIP5 Earth System Models, Global and Planetary Change, 150, 58-69, 2017.

Knorr, W., Jiang, L., and Arneth, A.: Climate, CO_2 and human population impacts on global wildfire emissions, Biogeosciences, 13, 267, 2016.

Lasslop, G., Thonicke, K., and Kloster, S.: SPITFIRE within the MPI Earth system model: Model development and evaluation, Journal of Advances in Modeling Earth Systems, 6, 740-755, 2014.

Laurent, P., Mouillot, F., Yue, C., Moreno, V., Ciais, P., and Nogueira, J.: Global fire patch properties derived from burned area products of the MODIS and MERIS space-borne instruments, Scientific Data, Doi: https://data.oreme.org/doi/view/0e999ffc-e220-41ac-ac85-76e92ecd0320, 2018 submitted.

Marlier, M. E., DeFries, R. S., Voulgarakis, A., Kinney, P. L., Randerson, J. T., Shindell, D. T., Chen, Y., and Faluvegi, G.: El Nino and health risks from landscape fire emissions in southeast Asia, Nature climate change, 3, 131-136, 2013.

Martín, M. P., Gómez, I., and Chuvieco, E.: Performance of a burned-area index (BAIM) for mapping Mediterranean burned scars from MODIS data, in: Proceedings of the 5th International Workshop on Remote Sensing and GIS applications to Forest Fire Management: Fire Effects Assessment, edited by: Riva, J., Pérez-Cabello, F., and Chuvieco, E., Universidad de Zaragoza, GOFC-GOLD, EARSeL, Paris, 193-198, 2005.

Mason, P., Zillman, J., Simmons, A., Lindstrom, E., Harrison, D., Dolman, H., Bojinski, S., Fischer, A., Latham, J., and Rasmussen, J.: Implementation plan for the global observing system for climate in support of the UNFCCC (2010 Update), 2010.

Moritz, M. A., Batllori, E., Bradstock, R. A., Gill, A. M., Handmer, J., Hessburg, P. F., Leonard, J., McCaffrey, S., Odion, D. C., and Schoennagel, T.: Learning to coexist with wildfire, Nature, 515, 58-66, 2014.

Mouillot, F., Schultz, M. G., Yue, C., Cadule, P., Tansey, K., Ciais, P., and Chuvieco, E.: Ten years of global burned area products from spaceborne remote sensing—A review: Analysis of user needs and recommendations for future developments, International Journal of Applied Earth Observation and Geoinformation, 26, 64-79, 2014.

Nogueira, J., Ruffault, J., Chuvieco, E., and Mouillot, F.: Can We Go Beyond Burned Area in the Assessment of Global Remote Sensing Products with Fire Patch Metrics?, Remote Sensing, 9, 7, 2017.

Olson, D. M., E. Dinerstein, E.D. Wikramanayake, N.D. Burgess, G.V.N. Powell, E.C. Underwood, J.A. D'amico, I. Itoua, H.E. Strand, J.C. Morrison, C.J. Loucks, T.F. Allnutt, T.H. Ricketts, Y. Kura, J.F. Lamoreux, W.W.Wettengel, P. Hedao, and K.R. Kassem: Terrestrial Ecoregions of the World: A New Map of Life on Earth, BioScience, 51, 933-938, 2001.

Padilla, M., Stehman, S. V., Hantson, S., Oliva, P., Alonso-Canas, I., Bradley, A., Tansey, K., Mota, B., Pereira, J. M., and Chuvieco, E.: Comparing the Accuracies of Remote Sensing Global Burned Area Products using Stratified Random Sampling and Estimation, RSE, 160, 114-121, Doi: http://dx.doi.org/10.1016/j.rse.2014.01.008, 2015.

Padilla, M., Olofsson, P., Stehman, S. V., Tansey, K., and Chuvieco, E.: Stratification and sample allocation for reference burned area data, RSE, 203, 240-255, Doi: doi.org/10.1016/j.rse.2017.06.041, 2017.

Padilla, M., Wheeler, J., and Tansey, K.: ESA CCI ECV Fire Disturbance Phase II: D4.1. Product Validation Report, in preparation.

Pereira, J. M. C.: A Comparative Evaluation of NOAA/AVHRR Vegetation Indexes for Burned Surface Detection and Mapping, IEEE Trans.Geos.R.S., 37, 217-226, 1999.

Pinty, B., and Verstraete, M. M.: GEMI: a non-linear index to monitor global vegetation from satellites, Vegetatio, 101, 15-20, 1992.

Plummer, S., Arino, O., Ranera, F., Tansey, K., Chen, J., Dedieu, G., Eva, H., Piccolini, I., Leigh, R., and Borstlap, G.: The GLOBCARBON Initiative: multi-sensor estimation of global biophysical products for global terrestrial carbon studies, Envisat & ERS Symposium, 2005,

Reid, C. E., Brauer, M., Johnston, F. H., Jerrett, M., Balmes, J. R., and Elliott, C. T.: Critical review of health impacts of wildfire smoke exposure, Environmental Health Perspectives, 124, 1334, 2016.

Román-Cuesta, R. M., Gracia, M., and Retana, J.: Factors influencing the formation of unburned forest islands within the perimeter of a large forest fire, Forest Ecol Manage, 258, 71-80, 2009.

Roos, C. I., Scott, A. C., Belcher, C. M., Chaloner, W. G., Aylen, J., Bird, R. B., Coughlan, M. R., Johnson, B. R., Johnston, F. H., and McMorrow, J.: Living on a flammable planet: interdisciplinary, cross-scalar and varied cultural lessons, prospects and challenges, Philosophical Transactions of the Royal Society B, 371, 20150469, 2016.

Roy, D., Jin, Y., Lewis, P., and Justice, C.: Prototyping a global algorithm for systematic fire-affected area mapping using MODIS time series data, RSE, 97, 137-162, 2005.

Roy, D. P., Boschetti, L., and Justice, C. O.: The collection 5 MODIS burned area product — Global evaluation by comparison with the MODIS active fire product, RSE, 112, 3690-3707, 2008.

Sturtevant, B. R., Miranda, B. R., Yang, J., He, H. S., Gustafson, E. J., and Scheller, R. M.: Studying fire mitigation strategies in multi-ownership landscapes: Balancing the management of fire-dependent ecosystems and fire risk, Ecosystems, 12, 445-461, 2009.

Tansey, K., Grégoire, J. M., Defourny, P., Leigh, R., Pekel, J. F., Van Bogaert, E., and Bartholomé, E.: A new, global, multi-annual (2000–2007) burnt area product at 1 km resolution, Geophysical Research Letters, 35, 2008.

van der Werf, G. R., Randerson, J. T., Giglio, L., van Leeuwen, T. T., Chen, Y., Rogers, B. M., Mu, M., van Marle, M. J. E., Morton, D. C., Collatz, G. J., Yokelson, R. J., and Kasibhatla, P. S.: Global fire emissions estimates during 1997–2015, Earth Syst. Sci. Data Discuss., 2017, 1-43, Doi: 10.5194/essd-2016-62, 2017.

Earth Syst. Sci. Data Discuss., https://doi.org/10.5194/essd-2018-46
Manuscript under review for journal Earth Syst. Sci. Data
Discussion started: 22 May 2018

Open Access Earth System Science Data Discussions

Table 1: Geographical distribution of BA tiles for the pixel product

Areas	Name	Upper left		Lower right	
1	North America	180°W	83°N	50°W	19°N
2	South America	105°W	19°N	34°W	57°S
3	Europe –North Africa	26°W	83°N	53°E	25°N
4	Asia	53°E	83°N	180°E	0°N
5	Sub-Saharan Africa	26°W	25°N	53°E	40°S
6	Australia & New Zealand	95°E	0°N	180°E	53°S

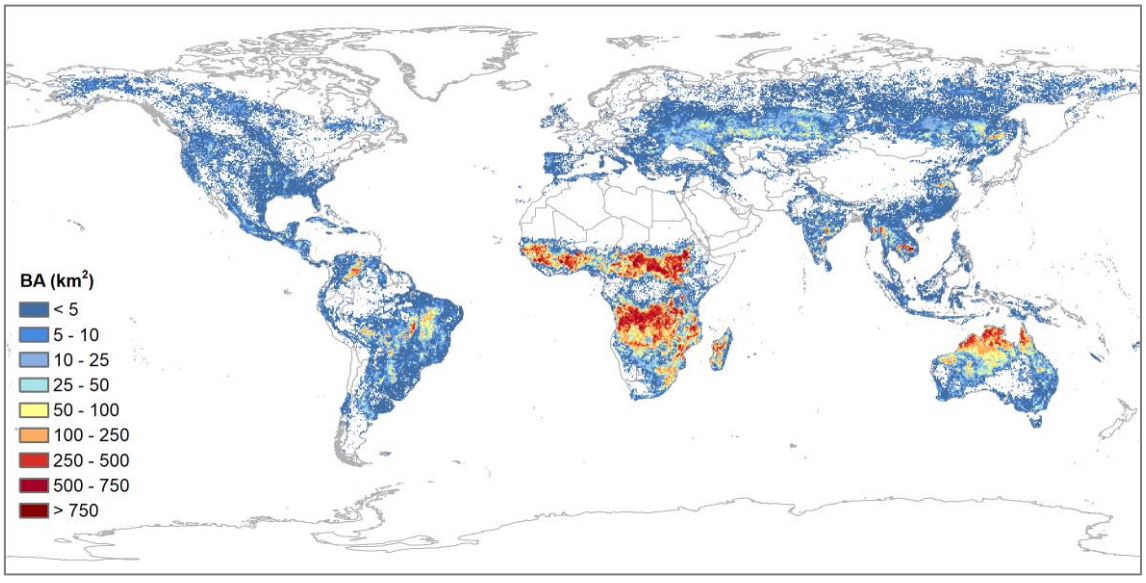

Figure 1: Average global annual BA from the MODIS Fire_cci v5.0 product

Earth Syst. Sci. Data Discuss., https://doi.org/10.5194/essd-2018-46
Manuscript under review for journal Earth Syst. Sci. Data
Discussion started: 22 May 2018

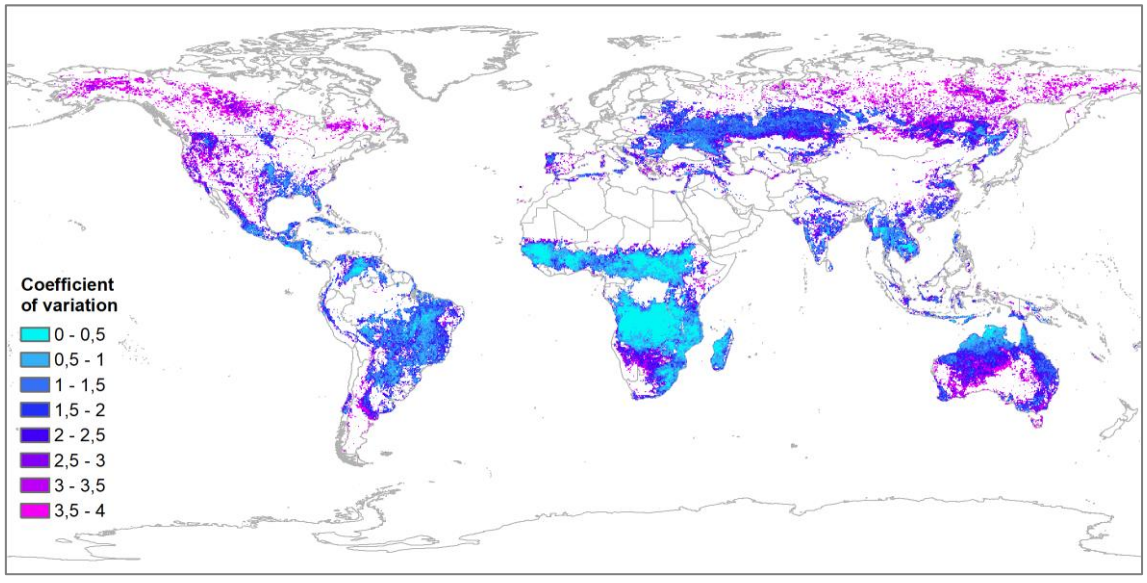

Figure 2: Coefficient of Variation of annual BA (2001-2016) for the MODIS Fire_cci v5.0 product

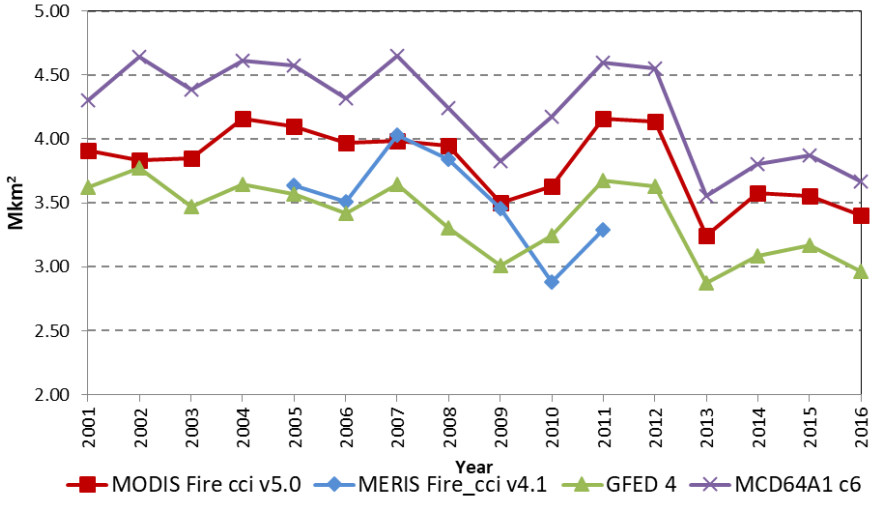

Figure 3: Temporal trends of yearly BA for different global products

Earth Syst. Sci. Data Discuss., https://doi.org/10.5194/essd-2018-46
Manuscript under review for journal Earth Syst. Sci. Data
Discussion started: 22 May 2018

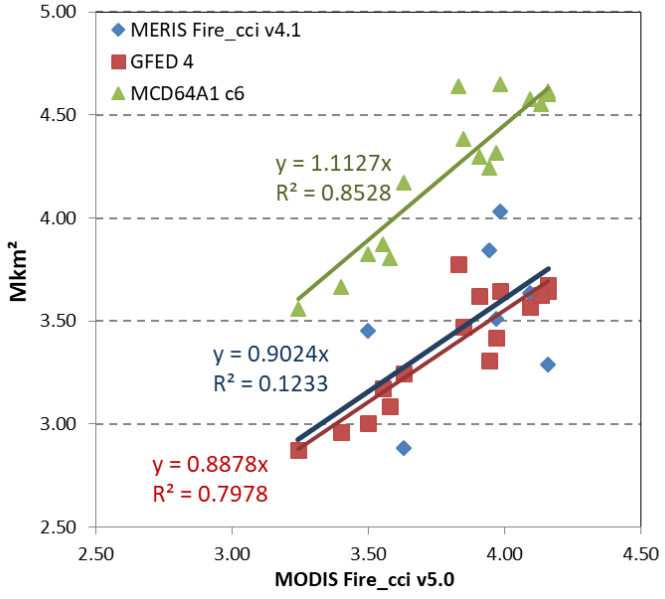

Figure 4: Regression analyses between the estimations of total BA of MODIS Fire_cci v5.0 and global existing BA products.

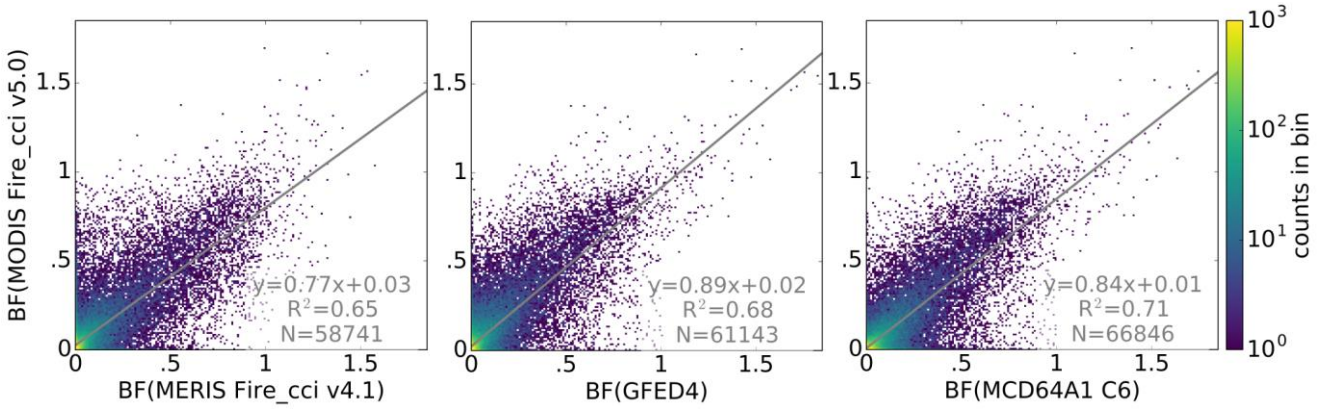

Figure 5: Two-dimensional histogram showing the relationship between global spatial patterns of gridded annual burned fraction (BF) in 2008 between MODIS Fire_cci v5.0 and in other global BA products (BF binned into increments of 0.02). Also shown is the result of the linear regression analyses.

Earth Syst. Sci. Data Discuss., https://doi.org/10.5194/essd-2018-46
Manuscript under review for journal Earth Syst. Sci. Data
Discussion started: 22 May 2018

Open Access Earth System Science Data Discussions

Table 2: Correlation matrix showing the coefficients of determination (r^2) calculated for different BA product pairs based on annual data (see Fig. 5). Given is the average and the range calculated from individual years in 2005-2011.

r^2 Mean (Min - Max)	MERIS Fire_cci v4.1	GFED4	MCD64A1 C6
MODIS Fire_cci v5.0	0.59 (0.44 - 0.65)	0.67 (0.64 - 0.69)	0.70 (0.68 - 0.72)
MERIS Fire_cci v4.1		0.47 (0.33 - 0.54)	0.49 (0.35 - 0.54)
GFED4			0.93 (0.92 - 0.94)

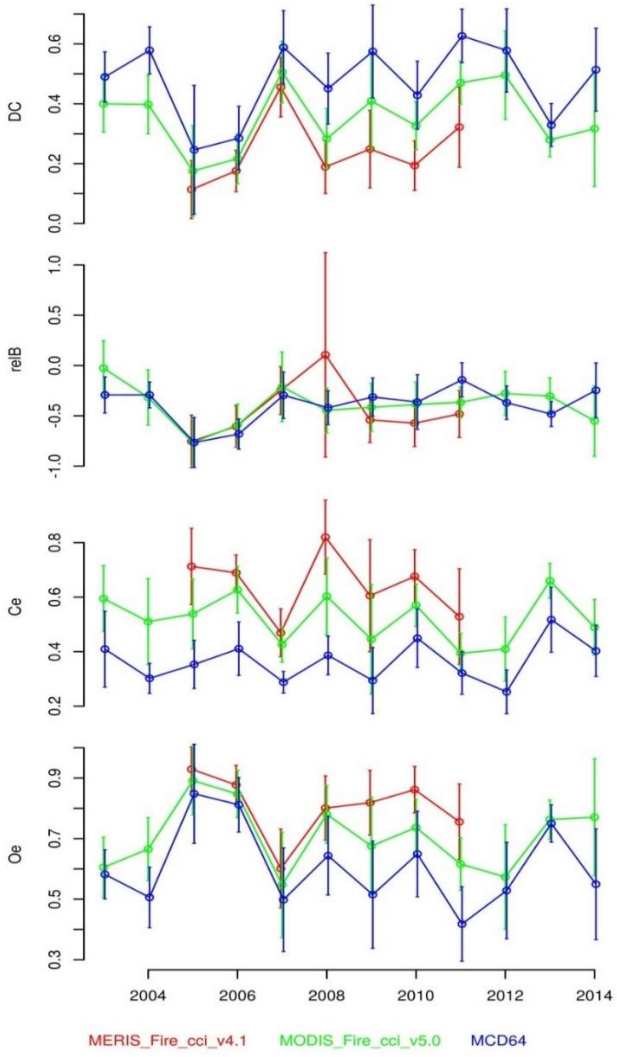

Figure 6: Estimates of Dice coefficient (DC), relative bias (relB), commission error ratio (Ce) and omission error ratio (Oe) at global scale and for each year. Vertical segments show the 95% confidence intervals. Points are slightly moved along the x-axis to improve visualization.

Earth Syst. Sci. Data Discuss., https://doi.org/10.5194/essd-2018-46
Manuscript under review for journal Earth Syst. Sci. Data
Discussion started: 22 May 2018

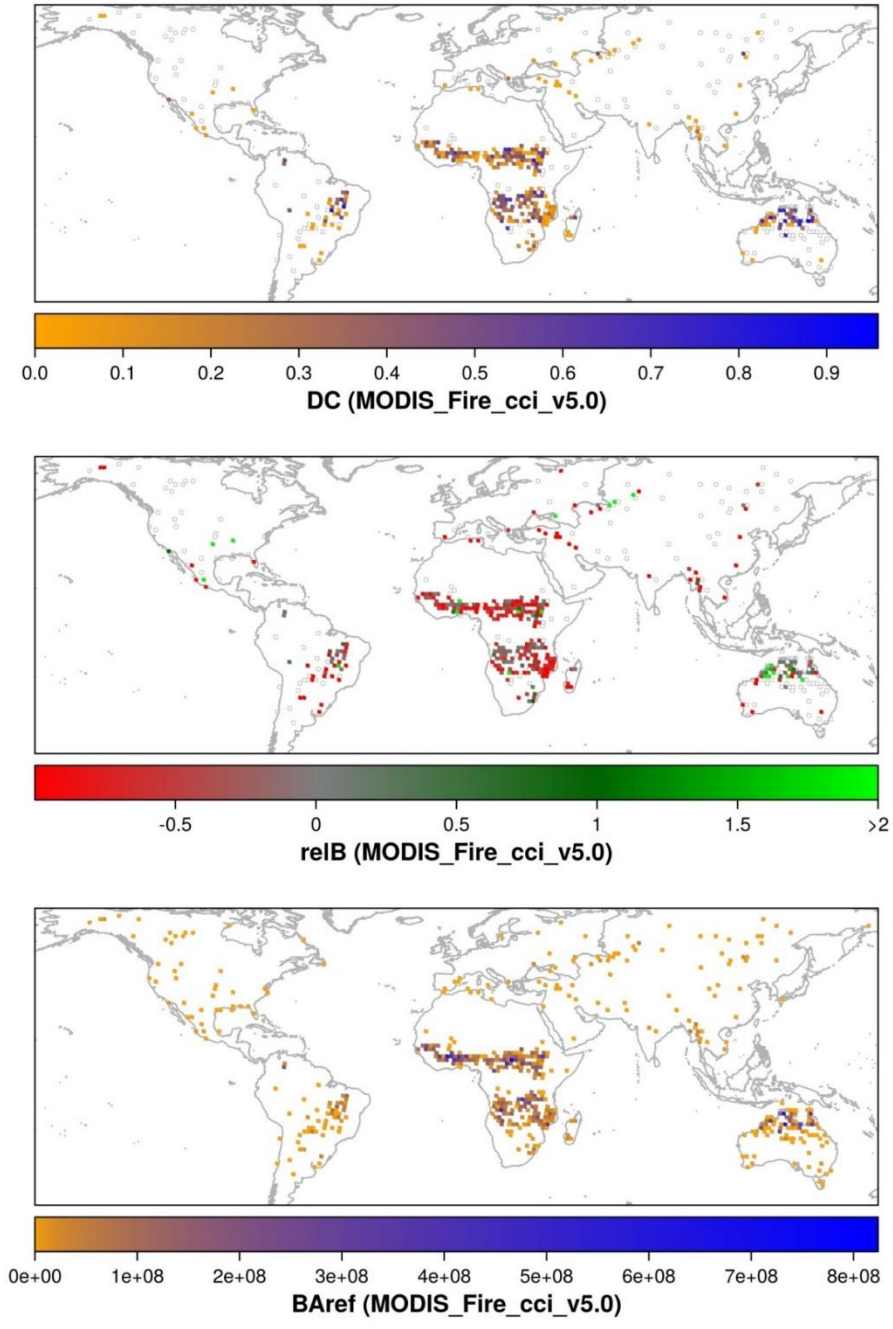

Figure 7: Dice of coefficient (DC), relative bias (relB) and reference burned area (BAref; m^2) for MODIS Fire_cci v5.0 at TSAs. TSAs with reference data but without accuracy measure available are represented by empty polygons (white polygons with grey borders). DC is not available when there is no BA in the reference data or in the product, and relB is not available when there is no BA in the reference data.

Earth Syst. Sci. Data Discuss., https://doi.org/10.5194/essd-2018-46
Manuscript under review for journal Earth Syst. Sci. Data
Discussion started: 22 May 2018

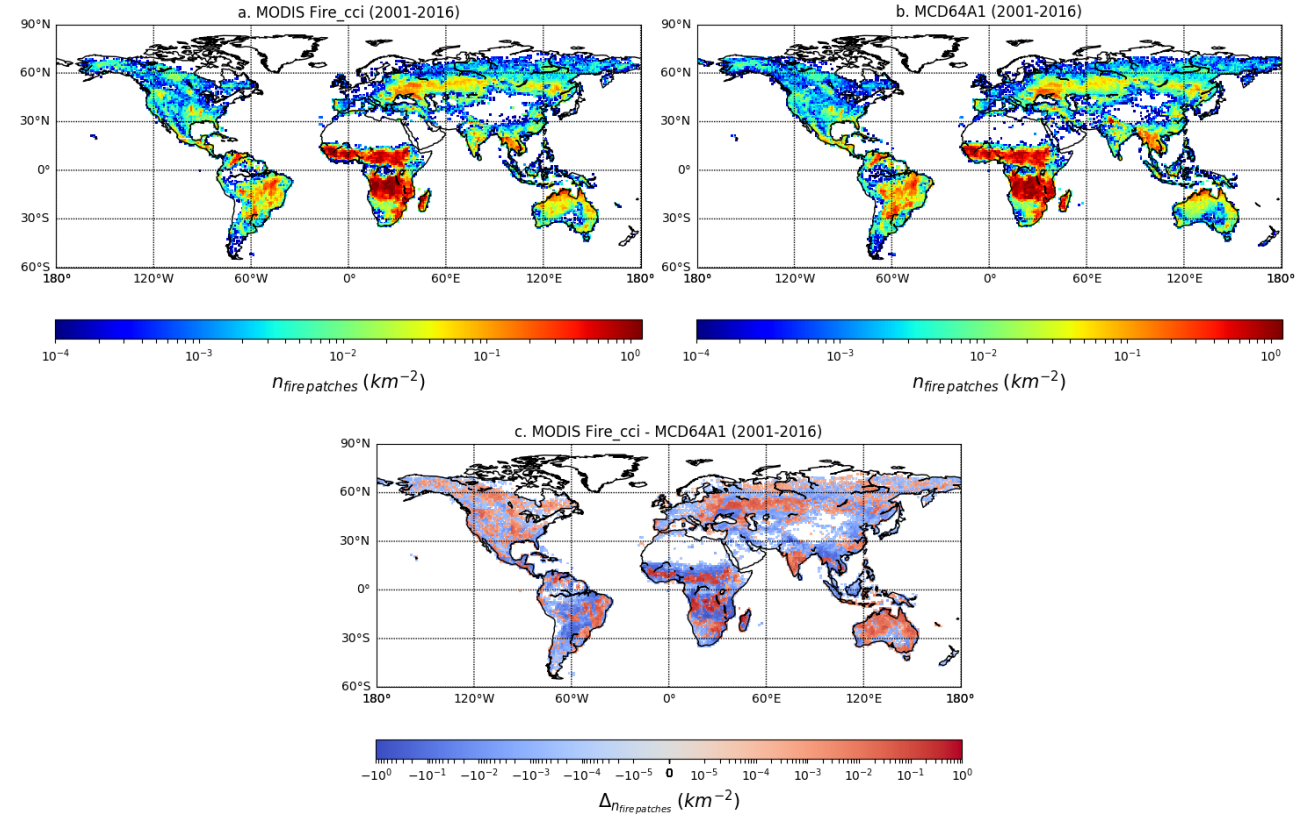

Figure 8: Global pattern of fire patch number (km^2) obtained from the pixel-level information of MODIS Fire_cci v5.0 (top left) and MCD64A1 c6 (top right) for the period 2000-2016. The difference between the two products is also presented (bottom). A minimum fire size of 107 ha has been chosen to prevent resolution effects.

Earth Syst. Sci. Data Discuss., https://doi.org/10.5194/essd-2018-46
Manuscript under review for journal Earth Syst. Sci. Data
Discussion started: 22 May 2018

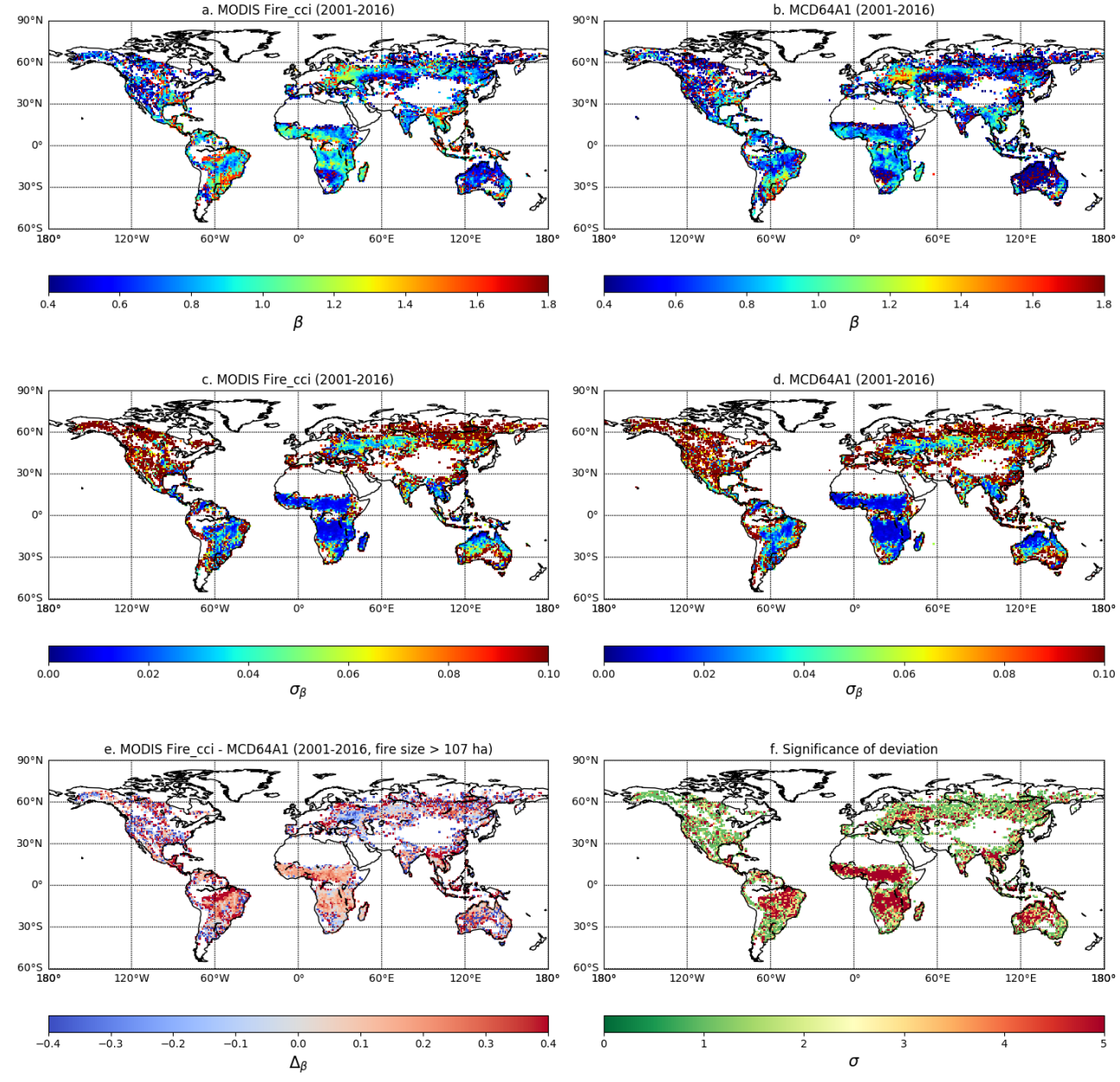

Figure 9: Slope (β) of the fire number/fire size relationship (log scale) and its uncertainty (σ) for MODIS Fire_cci v5.0 (top and middle left), MCD64A1 c6 (top and middle right). The difference between the two products is also presented (bottom left), with the level of agreement between the two products (bottom right).

Earth Syst. Sci. Data Discuss., https://doi.org/10.5194/essd-2018-46
Manuscript under review for journal Earth Syst. Sci. Data
Discussion started: 22 May 2018

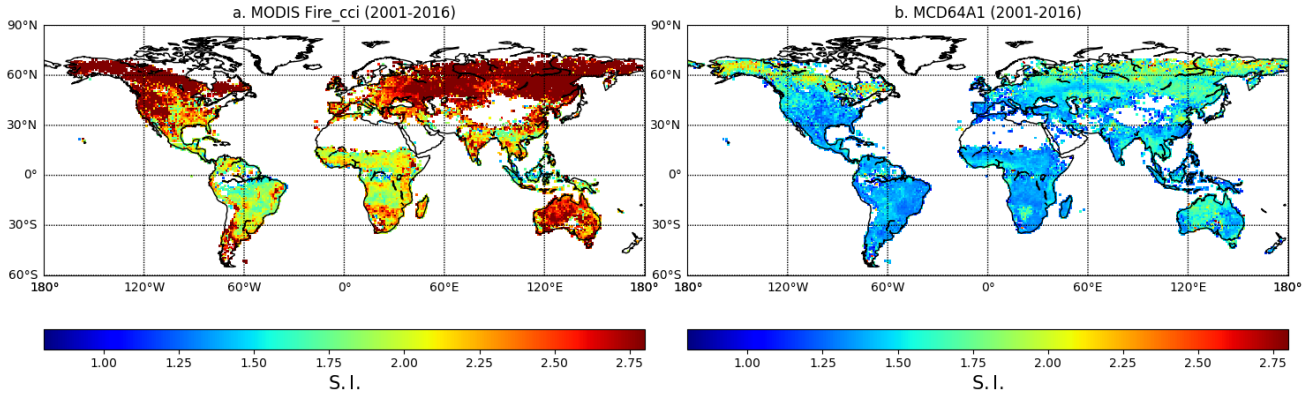

Figure 10: Shape Index for MODIS Fire_cci v5.0 (left) and MCD64A1 c6 (right).